Lawrence Berkeley National Laboratory

Title
Prediction of solubility parameters of lignin and ionic liquids using multi-resolution simulation approaches

Permalink
https://escholarship.org/uc/item/2h5785qx

Journal

ISSN

Authors
Mohan, Mood
Huang, Kaixuan
Pidatala, Venkataramana R
et al.

Publication Date

DOI

Copyright Information

Green Chemistry

Cutting-edge research for a greener sustainable future

Accepted Manuscript
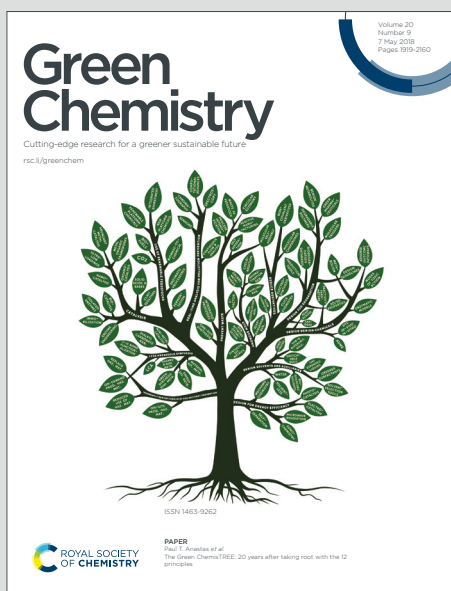
This is an Accepted Manuscript, which has been through the Royal Society of Chemistry peer review process and has been accepted for publication.

Accepted Manuscripts are published online shortly after acceptance, before technical editing, formatting and proof reading. Using this free service, authors can make their results available to the community, in citable form, before we publish the edited article. We will replace this Accepted Manuscript with the edited and formatted Advance Article as soon as it is available.

You can find more information about Accepted Manuscripts in the Information for Authors.

ROYAL SOCIETY
OF CHEMISTRY

rsc.li/greenchem

Prediction of Solubility Parameters of Lignin and Ionic Liquids Using Multi-resolution Simulation Approaches

Mood Mohan[1,2], Kaixuan Huang[1,3,4,5], Venkataramana Reddy Pidatala[1,3], Blake A. Simmons[1,3], Seema Singh[1,2], Kenneth Sale[*,1,6], and John Gladden[*,1,2]

[1] Deconstruction Division, Joint BioEnergy Institute, 5885 Hollis Street, Emeryville, California 94608, United States

[2] Department of Biomaterials and Biomanufacturing, Sandia National Laboratories, 7011 East Avenue, Livermore, California 94551, United States

[3] Biological Systems and Engineering Division, Lawrence Berkeley National Laboratory, 1 Cyclotron Road, Berkeley, California 94720, United States

[4] Key Laboratory of Forestry Genetics & Biotechnology (Nanjing Forestry University), Ministry of Education, Nanjing 210037, People's Republic of China

[5] College of Marine and Bio-engineering, Yancheng Teachers University, Yancheng, Jiangsu 224002, People's Republic of China

[6] Department of Computational Biology and Biophysics, Sandia National Laboratories, 7011 East Avenue, Livermore, California 94551, United States

[*]Corresponding Author

E-mail: *jmgladden@lbl.gov; jmgladd@sandia.gov* (J. M. Gladden)

klsale@lbl.gov, klsale@sandia.gov (Kenneth Sale)

Green Chemistry Accepted Manuscript

Abstract

The solubility parameter (SP) of a molecular species is a vital feature that evaluates polarity and quantifies the 'like-seeks-like' principle, which is used in chemistry to screen solvents for dissolution. Recent studies demonstrated that ionic liquids (ILs) and deep eutectic solvents (DESs) efficiently solubilize lignocellulosic biomass and promote enzymatic saccharification for production of sugars used for production of biofuels and value-added chemicals. Understanding the solubility of plant biopolymers, particularly lignin, in ILs and DESs is critical for selecting candidate ILs and DESs for biomass pretreatment; however, experimentally measuring SPs are challenging. Thus, the present study investigates lignin dissolution mechanisms in IL/DES and prediction of the solubility parameters (Hildebrand and Hansen) of lignin, ILs, and DESs using multi-resolution simulation approaches. Solubility parameters of studied compounds were predicted using molecular dynamics (MD) simulations, and the SPs of lignin were determined to be 23–27 MPa$^{1/2}$, which was close to the polymeric lignin solubility parameters (24.3–25.5 MPa$^{1/2}$). The SPs of ILs namely [Ch][Lys], [Ch][Oct], and [Emim][Lys] were predicted to be ~26 MPa$^{1/2}$, which is close to lignin's SPs and resulted in increased biomass delignification. The MD simulated SPs were validated by both the COSMO-RS model and experimental investigations, with the results showing a close agreement between predicted and experimental SPs. In addition, the enthalpy of vaporization (ΔH_{vap}) of the ILs/DESs was predicted based on the potential energy of the system, and the ΔH_{vap} of ILs/DESs was around 40-65 kcal/mol, which is 5-8 times higher than the traditional organic solvents.

1. Introduction

Lignin is one of the major constituents of lignocellulosic biomass along with cellulose and hemicellulose and is the most abundant known renewable source of aromatics.[1,2] It is a complex heterogeneous biopolymer composed of three major phenylpropane units: p-coumaryl, coniferyl, and sinapyl. These phenylpropane monomers are firmly bonded together by C–O–C ether (carbon-oxygen: β–O–4, α–O–4, and 4–O–5) and C–C interunit (β–β, β–5, β–1, and 5–5) bonds.[3-5] In lignin, β–O–4 bonds are the most ubiquitous ether linkage, accounting for 40-65 % of all inter-subunit linkages. Additionally, lignin contains a variety of functional groups, including methoxy, phenolics, aliphatic hydroxy, cyclic and noncyclic ethers, and carbonyl groups, all of which alter its polarity and reactivity.[3,6] The lignin structure is further complicated by H-bonds between neighboring O-containing groups and π-π interactions between aromatic moieties, which strengthen its recalcitrance to facile deconstruction.[7-9] Nevertheless, the utilization of lignin as a feedstock for the production of hydrocarbons and chemicals offers a significant opportunity for enhancing the overall operational efficiency, carbon conversion rate, economic viability, and sustainability of biorefinery processes.[2] Lignin solubilization and subsequent fractionation remains a key barrier for biorefineries due to its recalcitrance, heterogeneity, strong interactions, and hydrophobicity.[10] Hence, suitable solvents are required to enable lignin solubilization and separation.

Over the past few decades, ionic liquids (IL), organic salts with a melting temperature lower than 100 °C[11-13], have emerged as potent biomass solvents and have opened new opportunities for efficient (bio)polymer processing.[14-18] ILs exhibit several attractive properties such as having negligible vapor pressure, being non-flammable, non-toxic, high thermal and chemical stability, and acting as catalysts for specific reactions. Slight modifications to the structure of the cation and/or anion produces in an enormous range of potential ILs encompassing

a wide variety of solvent properties, and it has been demonstrated that the anion of IL plays a predominant role in the dissolution of (bio)polymers.[11,19] In another study, the alkyl chain length and the aromaticity of the IL cations were reported to have a significant effect on the dissolution of the biomass sugar polymers and lignin.[20] In addition to ILs, deep eutectic solvents (DES) have also emerged as green solvents and show numerous appealing properties like ILs, i.e., low vapor pressure, a wide range of liquid, good chemical and thermal stability, and excellent tunability.[21] DES are prepared by mixing two or more low-cost chemicals, which, in many cases, consist of a hydrogen bond acceptor (HBA) and a hydrogen bond donor (HBD) mixed at a specific molar ratio to turn them into a liquid state at room temperature.[22] IL-based and DES-based pretreatment solvents offer several advantages, including reducing biomass particle size, reduction of cellulose crystallinity, and selective extraction of lignin from biomass, thus enhancing fermentable sugar release.[14,23-25]

The interactions between different solvents and solute have been extensively studied to better understand how specific solvent-solute interactions and mixing processes influence solubility.[26-28] The activity coefficient and the Flory-Huggins interaction parameter are often used to quantify the interaction between solvent and solute when selecting the proper solvents for a specific application.[29,30] As an alternative, computing solubility parameters based on physical theory can be used to screen solvent systems for solubility of specific solutes. Hildebrand and Scott introduced the Hildebrand solubility parameter, which is an important physicochemical parameter and provides a reference in solvent selection and predicting material compatibility.[30] When the Hildebrand solubility parameter values of solute (e.g., lignin) and solvent (IL or DES) are close, solute is miscible in such solvents.[31,32] Hansen further refined the concept of Hildebrand solubility parameters with Hansen solubility parameters (HSP), where the Hildebrand value was broken

down into three contributing factors: i) dispersion forces, δ_d, ii) polarity, δ_p, and iii) hydrogen bonding, δ_h. The motivation for HSP was to quantify the miscibility and immiscibility patterns between the different chemical species.[30,33]

The performance of HSP model has previously been demonstrated for lignin solubility using different solvent systems.[29,31,34-36] Various methods are used to measure the solubility parameters of chemical species, such as swelling, group contribution method, inverse gas chromatography (IGC), and viscosity measurements.[30,34,37] Due to a large number of possible ILs and DESs and limited availability of experimental polarity data, it is not straightforward to select the best solvent for a specific application based on experimental measures. Hence, molecular simulation (e.g., molecular dynamics and continuum solvation models) provide a powerful approach to estimating the polarity of a solvent by the computation of the dispersion, polar, and hydrogen bonding contributions of the solubility parameters (SPs). Molecular simulations have indeed been used to compute the SPs of hybrid solvents (ILs, DESs, and organic solvents), pharmaceuticals, and (bio)polymers. Based on the reported lignin solubility parameter of 27.2-28 MPa[0.5] [38,39], Balaji *et al.* (2012)[32] and Wang *et al.* (2014)[38] screened various ILs for solubilization of lignin based on solubility parameters computed using COnductor like Screening MOdel for Real Solvents (COSMO-RS) model and IGC method, respectively. Hansen and Björkman[34] reported lignin solubility parameters of δ_p = 14.9 MPa$^{1/2}$, δ_h = 16.9 MPa$^{1/2}$, and δ_d = 21.9 MPa$^{1/2}$, while Thielemans and Wool (2005)[40] reported the HSP values of lignin were δ_p = 13.7 MPa$^{1/2}$, δ_h = 11.7 MPa$^{1/2}$, and δ_d = 16.7 MPa$^{1/2}$. Based on these studies, it should be noted that the HSP values cannot be assumed to be universal for all lignin samples and their delignification processes. Thus, an expansive chemical diversity between lignin from different sources in addition to the method of extraction of the lignin should provide other values for lignin.

Sun *et al.* (2014) investigated the pretreatment of switchgrass (grassy biomass) in imidazolium and cholinium-based ILs ([Emim][Lys], [Emim][OAc], [Ch][Lys], and [Ch][OAc]) both experimentally and computationally.[19] The computed strength of interaction energies between lignin and ILs were in the following order: [Ch][OAc] > [Emim][OAc] > [Ch][Lys] > [Emim][Lys], which were contrary to experimental delignification values. Dutta et al. (2018) studied the delignification of switchgrass (grass), eucalyptus (hardwood), and pine (softwood) in [Ch][Lys] and reported higher delignification of grassy and hardwood biomass than of softwood.[41] Based on these studies, the applicability of HSPs to delignification of different biomasses has remained questionable, and, to the best of our knowledge, the solubility parameters for grassy biomass have not yet been addressed. Hence, a systematic study of ILs for which biomass pretreatment data are available and that have shown promise in their ability to delignify biomass is needed and is the focus of the present work.

The present study evaluated the Hansen solubility parameters of lignin, ILs, and DESs using multi-resolution simulation approaches. We used molecular dynamics (MD) simulations to predict the solubility parameters of lignin, DESs, and various ILs. The COSMO-RS model and Hansen solubility parameters in practice (HSPiP) were employed to confirm the MD-derived solubility parameters and validate with experiments. Finally, the delignification of grassy biomass in different ILs and DESs was addressed and evaluated. The obtained results help to comprehend the dissolution of lignin in different solvent environments and to design a novel and effective solvent for delignification and viable biomass pretreatment.

2.   Computational Details

2.1.   Molecular Dynamics Simulations

The solubility parameter (δ) of a solvent is one of the critical properties that determine the polarity/non-polarity and quantifies the 'like-seeks-like' principle, which is often discussed in the

context of polymers dissolution.[30] The solubility parameters of investigated lignin, ILs, and DESs were calculated using the results from molecular dynamics (MD) simulations. The chemical structures of lignin polymers with different linkages, ILs (cations (cholinium, [Ch]$^+$ and 1-ethyl-3-methylimidazolium, [Emim]$^+$) and anions (formate [For]$^-$, acetate [Ace]$^-$, butyrate [But]$^-$, hexanoate [Hex]$^-$, octanoate [Oct]$^-$, lactate [Lac]$^-$, and lysinate [Lys]$^-$)), and metal-based deep eutectic solvents (mDESs: zinc chloride ethylene glycol (1:4) and zinc chloride glycerol (1:3)) were drawn using Avogadro[42] and are depicted in Figures 1-2 and Figures S1-S2. Herein, lignin polymeric structures contained all possible linkages with the degree of polymerization of 8, 11, and 26 were used as lignin model structures for all the MD simulations and the lignin polymers were parameterized and built using LigninBuilder.[43] The molecular geometries of all investigated molecules were optimized using *Gaussian09* with energies calculated at the B3LYP level of theory and 6-311+G(d,p) basis set. CHARMM36 force field parameters were employed for all the molecules in the MD simulations. Force field parameters for lignin polymers and [Emim][Ace] were taken from Vermaas *et al.* (2019)[43,44], and Mohan et al. (2017; 2018)[12,15], and the force field parameters for cholinium, formate, butyrate, hexanoate, octanoate, lactate, and lysinate were developed using the CGENFF tool.[45,46] Force field parameters of ILs were further validated by comparing MD-smiluated densities to their experimental densities. The deviation between predicted and experimental densities was less than 5% (Table S1). The CHARMM force field parameters for mDESs (ZnCl$_2$, ethylene glycol, and glycerol) were taken from the literature[45-47], and these force field parameters were also confirmed by comparing their calculated densities to experimental values. All MD simulations were carried out using the NAMD package[48] and were performed at constant temperature and pressure using the Langevin thermostat and Nose-Hoover Langevin barostat.[49,50] The initial configuration of mDESs (300 molecules) were prepared

according to the molar ratios of mDESs (i.e., $ZnCl_2$-EG (1:4) and $ZnCl_2$-Gly (1:3)) using

PACKMOL in a cubic box, and the bulk molecular mDES box corresponds to the liquid system.[51]

For MD simulations of the system involving $ZnCl_2$-EG (1:4) 300 molecules of $ZnCl_2$ were mixed

with 1200 molecules of ethylene glycol. Similarly, 300 molecules of $ZnCl_2$ were mixed with 900

molecules of glycerol to obtain a 1:3 molar ratio of $ZnCl_2$-Gly. Five hundred molecules of lignin

and ionic liquids were prepared to run the MD simulations.

Initially, the potential energy of the molecular system was minimized for 0.5 ns using the

steepest descent algorithm. After energy minimization, the system was gradually heated for 0.5 ns

in temperature increments of 0.001 K to a final temperature of 298.15 K. The system was

equilibrated at this temperature under the NPT ensemble for 5 ns, at which the volume of the

simulation box is fixed during the equilibration step and converged to its experimental condition

(stable density). Following equilibration, a 20 ns production phase was run under a constant NVT

ensemble. Further, the RDF plot of lignin/ILs/mDESs were plotted after equilibration and

production runs. The RDF plot of lignin/ILs/mDESs in both simulation runs are similar, thus, this

pattern also confirms the convergence of equilibration of the simulation system. The simulation

temperature was controlled using a damping coefficient of 1 ps^{-1}, and a damping factor of 50 fs

was used for pressure control with an oscillation period of 100 fs.[15,52] The Particle Mesh Ewald

(PME) method was implemented to treat long-range electrostatic interactions with an accuracy of

10^{-6} (PME tolerance) at a cut-off distance of 12 Å.[53]

The Hildebrand solubility parameter (δ) is defined as the square root of the cohesive energy

density (CED) and is derived from evaporation energy (i.e., the energy required to convert a liquid

to a gas).[54] To calculate the evaporation energy (ΔE_{vap}), knowledge of gas phase potential energy

is required.[26,55] Therefore, the gas phase MD simulations of investigated lignin, ILs, and DESs

were also performed. The initial configuration of the system for gas-phase simulations was generated by selecting three random individual lignin, IL, and mDES clusters from the final configuration of liquid simulations (size of the box was set to be the final volume of liquid simulation). Equilibration simulations for the gas phase system were run for 1 ns at 298.15 K under the NVT ensemble, and the production run lasted for 5 ns. A time step of 1 fs was used to integrate the equations of motion in the liquid phase simulations, whereas for the gas phase simulations, the time step was reduced to 0.1 fs to avoid disintegration of the clusters due to momentary repulsive forces. A cut-off distance of 12 Å was used, and the Particle Mesh Ewald (PME) method was implemented with an accuracy of 10^{-6}. At every 5 ps, the production data was saved for calculating the cohesive energy density (CED) and solubility parameter (δ) of the DESs.

2.2. Calculations of Solubility Parameters from MD simulations

As discussed, the Hildebrand solubility parameter is defined as the square root of the cohesive energy density:

$$\delta = \sqrt{CED} = \sqrt{\frac{\left(\Delta H_{vap} - RT \right)}{V_m}} \tag{1}$$

where ΔH_{vap} is the enthalpy of vaporization and V_m is the molar volume of the molecule. T and R are the temperature (in K) and universal gas constant (in kcal/K. mol).

The enthalpy of vaporization measures the interaction between anion and cations of IL, HBA, and HBD of DES, and self-favorable interactions within lignin in the bulk molecular system and is calculated according to the following equation.

$$\Delta H_{vap}\left(T\right) = H\left(p,T\right)_{gas} - H\left(p,T\right)_{box} = E_{gas} - E_{box} + p\left(V_{gas} - V_{box}\right)$$
$$\approx \left\langle PE_{gas} \right\rangle - \left(\frac{\left\langle PE_{box} \right\rangle}{N} \right) + RT \tag{2}$$

The terms gas and box correspond to the gas phase and bulk phase of the system. PE denotes the potential energy of the system and $\langle PE_{gas} \rangle$ is the average potential energy of the gas-phase (one IL/DES pair or one lignin molecule) of MD simulation system. $\langle PE_{box} \rangle$ is the average potential energy of the simulation box over the production phase of MD simulation system (last 20 ns). 'N' is the total number of molecules in the simulation box. The cohesive energy density can also be calculated as defined below[26]

$$CED = \frac{\left(\left(\frac{\langle PE_{box} \rangle}{N} \right) - \langle PE_{gas} \rangle \right)}{V_m} \tag{3}$$

The detailed information about the calculation of solubility parameters from MD simulations are reported elsewhere.[26,28,54]

2.3.   COSMO-RS Calculations

The COSMO-RS (**CO**nductor like **S**creening **MO**del for **R**eal **S**olvents) model is an alternative tool to connect both molecular and thermodynamic simulations. The COSMO-RS theory combines dielectric continuum solvation model COSMO with statistical thermodynamic conduct of interacting surfaces. The screening charge density distribution of sigma (σ–) moments is an excellent linear descriptor derived from linear regression models relating to the molecular properties.[56]

In the present study, COSMOquick was used to predict the Hansen solubility parameters (HSPs).[57] The COSMOquick program includes a massive database of quantum chemically calculated σ–profiles and uses an approximation of the σ–profiles by using molecular fragmentation. Here, the COSMO-RS model was used to predict the SPs of small molecules (lignin monomers, dimers, and trimers) and ionic liquids. First, the geometries of all the investigated

molecules such as lignin dimers, trimer, and ionic liquids were optimized at B3LYP/6-311+G(d,p)

level of theory and basis set. After optimization, the COSMO files were generated at the

BVP86/TZVP/DGA1 level of theory and basis set.[58-60] The generated COSMO files were then

used as an input in the COSMOquik (version 1.7, COSMOlogic, Leverkusen, Germany) package.

The calculation of HSP using COSMOquick is similar to virtual solubility screening in different

reference solvent systems. COSMOquick makes a primary guess for the partial solubility

parameters (δ_x) to compute the logarithmic activity coefficient (ln(ϒ)).

$$\ln\left(\gamma^x_{i,Hansen}\right) = \alpha \frac{V_x}{RT}\left[4\left(\delta_{d,x} - \delta_{d,i}\right)^2 + \left(\delta_{p,x} - \delta_{p,i}\right)^2 + \left(\delta_{h,x} - \delta_{h,i}\right)^2\right] \tag{4}$$

where x denotes the solute, i corresponds to a reference solvent, α is the universal (Hansen)

parameter, and V_x is the molar volume of the solute. Subsequently, the COSMO-RS derived

parameters are plugged into a sigmoid equation to differentiate suitable solvents (if f(x) ≈ 1) from

bad solvents (if f(x) ≈ 0). The solubility parameter optimization procedure minimized the squared

difference between the two functions (eqn (5))

$$\sum\left[f\left(\ln\left(\gamma^x_{i,Hansen}\right)\right) - f\left(\ln\left(\gamma^x_{i,COSMO-RS}\right)\right)\right]^2 = \min \tag{5}$$

As an alternative, COSMOquick uses the QSPR (Quantitative Structure Property Relation) method

to determine the solubility parameters. COSMOquick also uses sigma moments combined with an

artificial neural network model in combination with a random forest algorithm trained with

literature data.

3.   Materials and Methods

The IL cholinium lysinate ([Ch][Lys]) was synthesized in our lab following published

protocols.[61] The IL was purified before the experiments by freeze drier evaporation. A series of

different organic solvents were purchased from Sigma Aldrich and are used without any further

purification. The details of organic solvents and their HSP values are provided in Table S2 (supporting information).

3.1.   HSPiP Method for Determination of HSP

The program Hansen Solubility Parameters in Practice (HSPiP) was also employed to determine the HSP of lignin and [Ch][Lys] IL. For lignin (neutral molecule), the HSP values are calculated using simple molecular descriptors such as SMILES (Simplified Molecular Input Line Entry System) as an input. For ILs (charged molecules), it is not possible to calculate the solubility parameters using SMILES in HSPiP, thus, it has to perform the solubility experiments in order to determine the IL HSP values. The HSP of [Ch][Lys] was measured by calculating the solubility of [Ch][Lys] in 19 different organic solvents. For each solubility experiment, 0.5 mL of [Ch][Lys] was added into a test tube containing 5 mL of organic solvent. The mixture was stirred at room temperature for 2 h. After stirring, the solubility mixture was allowed to stand for 24 h, and the solubility was visually observed and recorded. After the solubility observations, the solvents were given scores based on their solubility. Good solvents (those which were dissolved) were given a "1" score, and bad solvents (those which were partially or (un)-dissolved) were given "0" score. The resulting experimental data was entered into the HSPiP (version 5.2.02) to obtain Hansen solubility parameters for [Ch][Lys].

4.   Results and Discussions

Based on the cohesive energy density assumptions, Hansen has decomposed the total solubility parameter (δ_t) into the three meaningful contributors, namely polar (δ_p), hydrogen-bonded (δ_h), and dispersion (δ_d) forces.[30]

$$\delta_t = \sqrt{\left(\delta_p^2 + \delta_h^2 + \delta_d^2 \right)}$$

(6)

However, in MD simulations, the force field parameters do not have an explicit hydrogen bonding term, which indicates that the polar and hydrogen bond contributions of HSP cannot be measured separately. For this reason, the polar and hydrogen-bonded parameter combined into a single electrostatic term, (δ_e):[28,54,55]

$$\delta_e = \sqrt{\delta_p^2 + \delta_h^2} \tag{7}$$

In addition to the total solubility parameter, Hansen developed a relative energy difference (RED) parameter, which relates the interaction between a solute and a solvent. The RED is defined as the ratio between the radius of interaction (R_a) to the 3D sphere radius of the solute (R_0) as shown in the below equations (8 and 9).[29,30,33,34]

$$R_a = \sqrt{4\left(\delta_p^{solute} - \delta_p^{solvent}\right)^2 + \left(\delta_h^{solute} - \delta_h^{solvent}\right)^2 + \left(\delta_d^{solute} - \delta_d^{solvent}\right)^2} \tag{8}$$

$$RED = \frac{R_a}{R_0} \tag{9}$$

If the RED < 1, then the affinity of the solvent towards the solute is said to be higher. While If the RED > 1, the affinity between the solvent and solute is lower.

4.1. Measurement of Solubility Parameters for Ionic Liquid and Eutectic Solvents

The Hansen solubility parameters (HSP) of ionic liquids (ILs) and metal-based deep eutectic solvents (mDESs) have been predicted and reported in Table 1. Table 1 also reports the molar heat of vaporization (ΔH_{vap}), cohesive energy density (CED), and Hildebrand solubility parameters (δ_H) of ILs and mDESs. First, we discuss the solubility parameters of carboxylate-anion based ILs namely [Ch][For], [Ch][Ace], [Ch][But], [Ch][Hex], and [Ch][Oct]. As the alkyl chain length of carboxylate anion increased from formate to octanoate, the value of solubility parameters decreased. This is explained by the fact that the anions with shorter alkyl chains have higher polarity than the longer alkyl chain length anions i.e., hexanoate and octanoate, thus leading

to higher solubility parameter values. On the other hand, the interaction energy between anions and the IL's cation is stronger in the shorter alkyl chains of anions than it is for the longer alkyl chains of anions.[62] The stronger interaction energy between anion and cation leads to the higher polarity of IL thus, the solubility parameters of [Ch][For] and [Ch][Ace] are larger than those of [Ch][Hex] and [Ch][Oct]. In contrast to solubility parameters, the longer alkyl chain of anions ([Hex]$^-$ and [Oct]$^-$) had higher heat of vaporization than shorter alkyl chain anions such as [Ace]$^-$ and [For]$^-$. The higher molar heat of vaporization of [Ch][Oct] and [Ch][Hex] is due to their bulky liquid structures and stronger van der Waals interactions. On the other hand, the solubility parameters of cholinium lactate [Ch][Lac] and cholinium lysinate [Ch][Lys] were also predicted and shown in Table 1. The solubility parameters of [Ch][Ace] and [Ch][Lac] are close to each other i.e., 32.46 and 33.3, respectively. However, the molar heat of vaporization for [Ch][Lac] is higher than it is for [Ch][Ace], which is due to the higher polarity of lactate and stronger interactions between anion and cation of [Ch][Lac]. The solubility parameter of [Ch][Lys] is 26.52 MPa$^{1/2}$, which is close to the solubility parameter [Ch][Oct]. The similar HSP values of [Ch][Lys] and [Ch][Oct] are due to the bulky structure of their anions. Moreover, the interaction energies between anion and cation of both ILs are similar.[62] The calculated ΔH_{vap} of ILs is around 40-45 kcal/mol, which is 4-5 times higher than the traditional organic solvents (the evaporation energy of water is 9.7 kcal/mol, and methanol is 8.8 kcal/mol).[26,63]

The HSP of imidazolium-based cation (i.e., 1-ethyl-3-methylimidazolium, [Emim]$^+$) with acetate and lysinate anion were also predicted (Table 1) using data from MD simulations. The solubility parameters of [Emim][Ace] and [Emim][Lys] are 33.38 MPa$^{1/2}$ and 26.03 MPa$^{1/2}$, respectively. These solubility parameters are similar to the values for [Ch][Ace] and [Ch]Lys] HSP. It was interesting to note that the anion of the IL played a predominant role in controlling

the solubility parameter values. A closer look at the dispersion term in acetate and lysinate-based ILs, the IL containing [Emim]$^+$, showed a slightly higher δ_d than [Ch]$^+$-based ILs. This is due to the larger vdW forces between [Emim]$^+$ cation and anions. Liu et al. (2010)[26] performed the molecular dynamics of pure [Emim][Ace] and IL-cellulose mixtures at 300 K. It has been reported that the Hildebrand solubility parameter of [Emim][Ace] was 35.22 MPa$^{1/2}$, which was consistent with our predictions (i.e., 33.60 MPa$^{1/2}$).

It is worth mentioning that predictions of thermodynamic properties from MD simulations are sensitive to the CGENFF parameters and the magnitude of their penalties. However, in this work, except for the lysinate anion, the penalties for all investigated ions ([Ch]$^+$, [Emim]$^+$, [For]$^-$, [Ace]$^-$, [But]$^-$, [Hex]$^-$, [Oct]$^-$, and [Lac]$^-$) were zero, and the penalties for the lysinate anion was 33. According to Vanommeslaeghe et al. (2012), penalties between 10 and 50 mean some basic validation is recommended but not necessary.[64,65] To validate the CGENFF generated force field parameters of lysinate-based ILs, we calculated the density and HSP of [Ch][Lys] and compared them to experimental values. The comparisons of MD predicted to experimental values of density and HSP are in excellent agreement (Table 1, 2, and S1). Also, in the present study, MD predicted total HSP value of [Emim][Ace] is also compared with literature (Liu et al.[26] used AMBER force field parameters for [Emim][Ace]), and the HSP values are almost in a similar range.

The MD simulated solubility parameters were further validated against both COSMO-RS model and experimental solubility parameters. The usability of the COSMO-RS model for the prediction of solubility parameters has been reported in the literature.[32,66] However, a separate benchmarking study has been performed for ionic liquids and common organic solvents to reproduce the experimental solubility parameter values. The experimental solubility parameter values of ionic liquids and common organic solvents were taken from the literature and the

summary of predicted solubility parameters is provided in Table S2 and Figure S3.   The results of solubility parameter validation show an excellent agreement between experimental, and COSMO-RS predicted HSPs of ionic liquids and molecular solvents. After extensive validation of HSPs of ILs, we then computed solubility parameters of cholinium-based ionic liquids. Table 1 reports the COSMO-RS predicted solubility parameters of [Ch][Lys] and [Ch][Lac] at room temperature. From Table 1, the agreement between MD simulated and COSMO-RS predicted solubility parameters was excellent, thus the MD simulated HSPs are validated with thermodynamic computation tools i.e., COSMO-RS model. In addition to MD simulation and COSMO-RS predictions, solubility parameters of [Ch][Lys] were validated with experimental data. As described in section 2.4., the experimental solubility of [Ch][Lys] in 19 different organic solvents was performed and the measured solubility data was used in the HSPiP program to derive HSP values (Table 1 and Table 2). From these experiments, the HSP value of [Ch][Lys] is 26.3 MPa$^{1/2}$ which is consistent with those derived from MD simulations based on potential energy values. Therefore, the MD simulation and COSMO-RS computation tools can be used to predict the solubility parameters of ILs as an alternative to experiments. Given the excellent agreement of HSP calculated from MD simulations with those calculated from COSMO-RS and with those measured experimentally, we were confidence our MD approach provides an approach for predicting HSP for a variety of solvent systems and, more importantly, a computationally efficient approach for predicting HSP of larger systems such as polymeric lignin that are beyond the size limits of what is reasonable to be efficiently calculated using COSMO-RS methods.

Recently, DESs gained attention as alternative solvents for pretreatment of lignocellulosic biomass.[67,68] However, the use of metal chloride-based DESs in the pretreatment of lignocellulosic biomass has not been studied, but we hypothesize these DESs have the potential to significantly

solubilize biomass. To investigate this hypothesis, the solubility parameters of mDESs were calculated using the MD simulation approach (Table 1). The mDES composed of zinc chloride ($ZnCl_2$) as hydrogen bond acceptor (HBA) and ethylene glycol (EG) and glycerol (Gly) as hydrogen bond donors (HBD) form eutectic mixtures at 1:4 and 1:3 molar ratio of HBA to HBD, respectively. The solubility parameter of $ZnCl_2$-EG (28.56 $MPa^{1/2}$) is lower than the parameter for $ZnCl_2$-Gly (31.53 $MPa^{1/2}$). The higher HSP value for $ZnCl_2$-Gly indicates $ZnCl_2$-Gly is more polar than $ZnCl_2$-EG and that the interaction between $ZnCl_2$ and glycerol (Gly) is stronger than $ZnCl_2$-EG (see δ_p values of DESs in Table 1 for polarity). On the other hand, the calculated ΔH_{vap} of mDESs are slightly higher than the ionic liquids (~1.2-1.4 times) and 6–7 times higher than the traditional organic solvents.

4.2.   Measurement of Lignin Solubility Parameters

The Hansen solubility parameters (HSP) of lignin polymeric structures were calculated using the MD simulation approach. Model polymeric structures of lignin with degree of polymerization 8, 11 and 26 (DP = 8, 11, 26; Figure 1) were generated using LigninBuilder tool[43] and HSP values calculated using MD simulations (Table 3). The higher DP lignin molecule represents a more natural lignin due to the presence of all lignin linkages among the different monomeric units. From Table 3, the total solubility parameters of the various lignin polymers were predicted to be 23–27 $MPa^{1/2}$, which is close to the polymeric lignin solubility parameters (24.3-25.5 $MPa^{1/2}$).[40,69] As the degree of polymerization of lignin increased, the solubility parameters of lignin decreased; however, the difference in HSP values are minimal from DP = 8 to 26. It is interesting to observe that as the degree of polymerization of lignin increases, the contribution of the dispersion term to the total HSP was higher than the electrostatic (i.e., polar and hydrogen) term. This higher value of dispersion parameter is obtained due to the higher aromaticity and stronger hydrophobic sites

of lignin. Experimental HSP values of lignin are 25.50 MPa$^{1/2}$, 24.30 MPa$^{1/2}$, and 31.05 MPa$^{1/2}$ for organosolv lignin, hardwood kraft lignin, and extracted wood lignin, respectively. Apart from extracted wood lignin and lignin polymer with DP = 8 solubility parameters, all other predicted lignin solubility parameters are in a similar assortment (23-25 MPa$^{1/2}$). The lignin polymer with DP = 8 contains ~43% of C-C linkages which is close to softwood lignin linkage composition, and thus produced higher HSP values. Further, the solubility parameters of lignin monomers, dimers, and trimers were predicted using the COSMO-RS model (Table S3). From Table S3, the solubility parameters of C–C (5–5, β–5, β–1, and β–β) linkage lignin molecule had higher HSP values than ether linked lignin molecules. The applicability of lignin solubility parameters for different biomasses, as well as assessing the competence of ILs/DESs for lignin removal will be explored in the next section.

4.3. Lignin Removal based on the Solubility Parameters

Hansen Solubility parameters were introduced to develop an approach to rapidly screen for a suitable solvent for polymer dissolutions as well as drug solubility.[30,33] These HSPs can also be used to screen solvents for lignin dissolution and lignocellulosic biomass delignification by looking for solvent–biomass combinations with similar HSPs. There are several literature reports on the delignification of biomass using ionic liquids and deep eutectic solvents.[14,38,67,68,70] Therefore, we explored Hansen solubility parameters as a tool to understand the delignification of biomass in ILs/DESs. Recently, Achinivu et al. (2021) studied the delignification of sorghum biomass using different molecular solvents such as amines and organic solvents.[71] Hansen and Björkman reported lignin solubility parameters (δ_p = 14.9 MPa$^{1/2}$, δ_h = 16.9 MPa$^{1/2}$, and δ_d = 21.9 MPa$^{1/2}$) do not correlate with experimental delignification. However, Thielemans and Wool (2005)[40] reported HSP values of lignin (δ_p = 13.5 MPa$^{1/2}$, δ_h = 11.3 MPa$^{1/2}$, and δ_d = 16.7 MPa$^{1/2}$)

correlated with biomass delignification results using amines and organic solvents. Therefore, it should be noted that the HSP values cannot be assumed universally for all lignin samples and their delignification processes, and an excessive chemical diversity among lignin variants from different sources in addition to the method of extraction of the lignin should provide other values for lignin. It has also been demonstrated that amines with δ_t = 22-24 MPa$^{1/2}$ were predicted to be effective solvents for lignin removal. Thus, we use Thielemans and Wool (2005) [40] reported HSP values for lignin (δ_p = 13.5 MPa$^{1/2}$, δ_h = 11.3 MPa$^{1/2}$, and δ_d = 16.7 MPa$^{1/2}$) to understand the biomass delignification in ILs and DESs.

Hou et al. reported the experimental dissolution of lignin in [Ch]-carboxylate anion ILs and showed that [Ch][Oct] and [Ch][Hex] had higher lignin dissolution capability compared to [Ch][For], [Ch][Ace], and [Ch][But].[25] These experimental findings are in line with our predicted solubility parameters in which [Ch][Oct] and [Ch][Hex] shows lower RED values of lignin than [Ch][For], [Ch][Ace], and [Ch][But] (Table 4). In addition to solubility parameters, the stronger vdW interaction energies and longer H-bonding lifetimes of [Ch][Oct] and [Ch][Hex] with lignin lead to higher lignin dissolution.[62] Yao et al. studied the pretreatment of sorghum and its delignification using cholinium-based ILs ([Ch][Ace], [Ch][Oct], and [Ch][Lys]).[72] It was observed that [Ch][Lys] resulted in higher delignification (77%) than [Ch][Oct] (51.86%) and [Ch][Ace] (45%). A closer look at the RED values of [Ch][Lys] and [Ch][Oct] with lignin (Table 4), [Ch][Oct] had a marginally lower RED value than [Ch][Lys]; however, [Ch][Lys] yields higher biomass delignification. This ascription can be further explained by the number of hydrogen bonds, viscosity, and dissociation constant (pK$_a$) of ILs. Mohan et al. (2021) studied the dissolution mechanism of lignin in cholinium-based ILs by molecular dynamics simulations.[62] It was observed that [Ch][Lys] forms multiple hydrogen bonds with lignin molecules, thereby resulting in higher

biomass delignification. On the other hand, the higher removal of lignin in [Ch][Lys] may also be due to the lower viscosity of [Ch][Lys] and higher pK_a values of lysinate anions. The higher pK_a of lysinate (2.74 (COOH), 9.44 (α-NH_3^+), and 10.29 (ϵ-NH_3^+)) are able to deprotonate the lignin with a pK_a value up to 10.3, which implies a maximum charge density and higher delignification.

In another study, Sun et al. (2014)[19] investigated pretreatment of switchgrass using four different ionic liquids, [Emim][Lys], [Emim][Ace], [Ch][Lys], and [Ch][Ace], by both experimental and computational approaches. They reported that lysinate-based ILs yielded higher biomass delignification (70-87%) than acetate-based ILs. They calculated the interaction energies between lignin and the four ILs using quantum chemical methods and arranged in the following order: [Ch][Ace] > [Emim][Ace] > [Ch][Lys] > [Emim][Lys], which were not consistent with experimental lignin removal. However, the current study predicted solubility parameters that show good correlation with experimental lignin removal. Lysinate-based ILs had showed lower RED values for lignin than acetate-based ILs and the order of RED values was: [Emim][Lys] > [Ch][Lys] > [Ch][Ace] > [Emim][Ace], which is in excellent agreement with experimental delignification. Hence, the solubility parameters provide useful insight in understanding biomass delignification efficacy. Dutta et al. (2018)[41] investigated delignification of grass, hardwood, and softwood biomasses using [Ch][Lys] IL. Grass and hardwood biomass results in higher biomass delignification (70-74%) than softwood biomass (20%). From the HSP point of view, grass and hardwood biomasses have lower RED values, and softwood biomass exhibits a higher RED value of lignin (Table 4). The higher removal of lignin from hardwood and grassy biomasses in [Ch][Lys] is due to the presence of larger amounts of ether linkages 60-80%.[10,73] These ether linkages are highly solvated by [Ch][Lys] when compared to C-C linkages (softwood biomass).[62] The main structural differences between these three types of lignin are a lower content of free

phenolic hydroxyl groups. Substantially lower content of methoxyl groups is found in softwood and higher in hardwood/grass lignins, and the hardwood/grass lignins are less cross-linked than the softwood lignins.[74,75]

Recently, we used a protic ionic liquid (ethanolamine acetate [EOA][Ace]) to study the delignification mechanism of poplar biomass.[55] Protic ionic liquids (PILs) are simply derived from mixing a Brønsted acid with a Brønsted base, resulting in the formation of individual ions. However, in general, various factors influence proton transfer and complete proton transfer is highly improbable. As a result, both ionic and neutral species co-exist, and the favorability of proton transfer of acid (acetic acid) and base (ethanolamine) was found to be incomplete, confirming the presence of neutral species in the mixture. The HSP value of neutral species ($\delta_t =$ 26.15 MPa$^{1/2}$) of [EOA][OAc] is closer to lignin (RED = 0.28) than for the ionic species ($\delta_t =$ 42.02 MPa$^{1/2}$ and RED = 1.52), resulting in 35-45% lignin removal. When dealing with protic ionic liquids, it is important to note that the favorability of proton transfer between acid and base of PILs should be measured to understand the stability of PILs and then calculate the desired thermodynamic properties for precisely unveiling the lignin removal mechanism.

As discussed earlier, metal-based DESs have gained significant attention as solvents for deconstruction of lignocellulosic biomass, and we hypothesized that the investigated mDESs have potential capability to solubilize lignin. Recently, Das et al. (2021) studied the effects of mDESs on pretreatment of sorghum and observed that $ZnCl_2$-EG solvated and extracted lignin and resulted in higher sugar yields compared to pretreatment with $ZnCl_2$-Gly.[76] The higher lignin extraction directly correlated with an increase in enzymatic saccharification efficiency (sugar yield) of pretreated lignocellulose.[71] From HSP point of view, $ZnCl_2$-EG had a lower RED of lignin (RED = 0.48) than $ZnCl_2$-Gly (0.75), indicating stronger interaction energies between lignin and $ZnCl_2$-

EG and predicting that $ZnCl_2$-EG would efficiently extract lignin from biomass and result in higher sugar yields, which is in agreement with the results of Das et al..[76] Based on the solubility parameters of lignin, it was also speculated that both vdW and electrostatic interactions played a predominate role in the dissolution of lignin, whereas in the case of cellulose and hemicellulose, the electrostatic interactions govern the dissolution process in ILs/DES.

5.   Conclusions

The current study attempts to understand the dissolution mechanism of lignin in ionic liquids and deep eutectic solvents by predicting the solubility parameters (SPs) using multi-resolution molecular simulation strategies. The MD simulations and COSMO-RS model has been employed to predict the solubility parameters of lignin, ILs, and DESs and validated with experimental investigations. The SPs of lignin were obtained in the range of 23–27 $MPa^{1/2}$, which is close to the polymeric lignin solubility parameters. Further, the correlation between experimental lignin dissolution in ILs and DESs and predicted REDs of lignin had shown an excellent agreement. The ILs with closer solubility parameter values of lignin are said to be better solvents for lignin removal and [Ch][Lys] was found to be a better solvent for lignin. It was also worthwhile to mention that the predicted solubility parameters were applicable for hardwood and grassy-type biomass, whereas the softwood biomass has a different set of SPs for lignin. Thus, the removal of lignin in hardwood and grassy-type biomasses are higher and similar, where the removal of lignin in softwood is much lower. The structural differences between these three types of lignin are a lower content of free phenolic hydroxyl groups. Softwood lignin is more polar and higher reactive (less methoxy groups and higher hydroxyl groups) than hardwood and grass lignin.

Acknowledgments

Supporting Information

The molecular structures of lignin polymers, MD predicted densities of ionic liquids/DES, and the COSMO-RS predicted HSPs of molecular solvents, ILs, and lignin compounds are presented in the supporting information along with this manuscript.

AUTHOR INFORMATION

Corresponding Authors

* E-mail: jmgladden@lbl.gov, jmgladd@sandia.gov (John M. Gladden);

klsale@lbl.gov, klsale@sandia.gov (Kenneth Sale)

ORCID

Mood Mohan   https://orcid.org/0000-0001-5937-9746

Kaixuan Huang   https://orcid.org/0000-0003-1731-907X

Venkataramana R. Pidatala   https://orcid.org/0000-0003-2637-3983

Blake A. Simmons   https://orcid.org/0000-0002-1332-1810

Seema Singh   https://orcid.org/0000-0002-1027-2697

Kenneth Sale   https://orcid.org/0000-0002-4269-8940

John M. Gladden   https://orcid.org/0000-0002-6985-2485

Notes

The authors declare no competing financial interest.

References

1. I. Cesarino, P. Araújo, A. P. Domingues Júnior and P. Mazzafera, *Braz. J. Bot.*, 2012, **35**, 303-311.
2. W. G. Glasser, *Frontiers in chemistry*, 2019, **7**, 565.
3. Z.-H. Liu and J. S. Yuan, in *Lignin Valorization*, 2018, pp. 314-332.
4. C. Xu and F. Ferdosian, in *Conversion of Lignin into Bio-Based Chemicals and Materials*, Springer, 2017, pp. 13-33.
5. R. Vanholme, B. Demedts, K. Morreel, J. Ralph and W. Boerjan, *Plant physiology*, 2010, **153**, 895-905.
6. Z. Fang and R. L. Smith Jr, *Production of biofuels and chemicals from lignin*, Springer, 2016.
7. Y. Zhang, H. He, K. Dong, M. Fan and S. Zhang, *RSC Adv.*, 2017, **7**, 12670-12681.
8. B. G. Janesko, *Phy. Chem. Chem. Phy.*, 2011, **13**, 11393-11401.
9. X. Qiu, Q. Kong, M. Zhou and D. Yang, *J. Phy. Chem. B*, 2010, **114**, 15857-15861.
10. L. Longe, G. Garnier and K. Saito, in *Production of Biofuels and Chemicals from Lignin*, Springer, 2016, pp. 147-179.
11. M. Mohan, C. Balaji, V. V. Goud and T. Banerjee, *J. Solution Chem.*, 2015, **44**, 538-557.
12. M. Mohan, T. Banerjee and V. V. Goud, *ChemistrySelect*, 2016, **1**, 4823-4832.
13. J. P. Hallett and T. Welton, *Chem. Rev.*, 2011, **111**, 3508-3576.
14. M. Mohan, N. N. Deshavath, T. Banerjee, V. V. Goud and V. V. Dasu, *Ind. Eng. Chem. Res.*, 2018, **57**, 10105-10117.
15. M. Mohan, P. Viswanath, T. Banerjee and V. V. Goud, *Mol. Phys.*, 2018, **116**, 2108-2128.
16. R. P. Swatloski, S. K. Spear, J. D. Holbrey and R. D. Rogers, *J. Am. Chem. Soc.*, 2002, **124**, 4974-4975.
17. Y. Li, J. Wang, X. Liu and S. Zhang, *Chem. Sci.*, 2018, **9**, 4027-4043.
18. M. J. Liszka, A. Kang, N. M. Konda, K. Tran, J. M. Gladden, S. Singh, J. D. Keasling, C. D. Scown, T. S. Lee and B. A. Simmons, *Green Chem.*, 2016, **18**, 4012-4021.
19. N. Sun, R. Parthasarathi, A. M. Socha, J. Shi, S. Zhang, V. Stavila, K. L. Sale, B. A. Simmons and S. Singh, *Green Chem.*, 2014, **16**, 2546-2557.
20. K. S. Khoo, X. Tan, C. W. Ooi, K. W. Chew, W. H. Leong, Y. H. Chai, S.-H. Ho and P. L. Show, *Journal of Cleaner Production*, 2021, **284**, 124772.
21. R. Verma, M. Mohan, V. V. Goud and T. Banerjee, *ACS Sustain. Chem. Eng.*, 2018, **6**, 16920-16932.
22. R. Wang, T. Wang, G. Yu and X. Chen, *Polymer Degradation and Stability*, 2021, **183**, 109463.
23. S. H. Lee, T. V. Doherty, R. J. Linhardt and J. S. Dordick, *Biotechnol. Bioeng.*, 2009, **102**, 1368-1376.
24. X. D. Hou, T. J. Smith, N. Li and M. H. Zong, *Biotechnol. Bioeng.*, 2012, **109**, 2484-2493.
25. X. D. Hou, J. Xu, N. Li and M. H. Zong, *Biotechnol. Bioeng.*, 2015, **112**, 65-73.
26. H. Liu, K. L. Sale, B. M. Holmes, B. A. Simmons and S. Singh, *J. Phy. Chem. B*, 2010, **114**, 4293-4301.
27. J. Guo, D. Zhang, C. Duan and C. Liu, *Carbohydrate research*, 2010, **345**, 2201-2205.
28. J. Gupta, C. Nunes, S. Vyas and S. Jonnalagadda, *J. Phy. Chem. B*, 2011, **115**, 2014-2023.
29. H. Yu, J. Hu and J. Chang, *Ind. Eng. Chem. Res.*, 2011, **50**, 7513-7519.
30. C. M. Hansen, *Hansen solubility parameters: a user's handbook*, CRC press, 2007.

Green Chemistry Accepted Manuscript

31. P. Weerachanchai, Z. Chen, S. S. J. Leong, M. W. Chang and J.-M. Lee, *Chemical engineering journal*, 2012, **213**, 356-362.

32. C. Balaji, T. Banerjee and V. V. Goud, *J. Solution Chem.*, 2012, **41**, 1610-1630.

33. C. M. Hansen, *Journal of Paint Technology*, 1967, **39**, 104-117.

34. C. Hansen and A. Björkman, *Holzforschung-International Journal of the Biology, Chemistry, Physics and Technology of Wood*, 1998, **52**, 335-344.

35. Q. Zhang, X. Tan, W. Wang, Q. Yu, Q. Wang, C. Miao, Y. Guo, X. Zhuang and Z. Yuan, *ACS Sustain. Chem. Eng.*, 2019, **7**, 8678-8686.

36. W. C. Ribeiro, P. F. M. Martinez and V. Lobosco, *BioResources*, 2020, **15**, 8577.

37. K. Adamska and A. Voelkel, *International journal of pharmaceutics*, 2005, **304**, 11-17.

38. Y. Wang, L. Wei, K. Li, Y. Ma, N. Ma, S. Ding, L. Wang, D. Zhao, B. Yan and W. Wan, *Bioresource technology*, 2014, **170**, 499-505.

39. J. Zhao and R. M. Wilkins, *J. Agric. Food Chem.*, 2000, **48**, 3651-3661.

40. W. Thielemans and R. P. Wool, *Biomacromolecules*, 2005, **6**, 1895-1905.

41. T. Dutta, G. Papa, E. Wang, J. Sun, N. G. Isern, J. R. Cort, B. A. Simmons and S. Singh, *ACS Sustain. Chem. Eng.*, 2018, **6**, 3079-3090.

42. M. D. Hanwell, D. E. Curtis, D. C. Lonie, T. Vandermeersch, E. Zurek and G. R. Hutchison, *J. Cheminformatics*, 2012, **4**, 17.

43. J. V. Vermaas, L. D. Dellon, L. J. Broadbelt, G. T. Beckham and M. F. Crowley, *ACS Sustain. Chem. Eng.*, 2018, **7**, 3443-3453.

44. J. V. Vermaas, L. Petridis, J. Ralph, M. F. Crowley and G. T. Beckham, *Green Chem.*, 2019, **21**, 109-122.

45. K. Vanommeslaeghe, E. Hatcher, C. Acharya, S. Kundu, S. Zhong, J. Shim, E. Darian, O. Guvench, P. Lopes and I. Vorobyov, *Journal of computational chemistry*, 2010, **31**, 671-690.

46. W. Yu, X. He, K. Vanommeslaeghe and A. D. MacKerell Jr, *Journal of computational chemistry*, 2012, **33**, 2451-2468.

47. R. H. Stote and M. Karplus, *Proteins: Structure, Function, and Bioinformatics*, 1995, **23**, 12-31.

48. J. C. Phillips, R. Braun, W. Wang, J. Gumbart, E. Tajkhorshid, E. Villa, C. Chipot, R. D. Skeel, L. Kale and K. Schulten, *Journal of computational chemistry*, 2005, **26**, 1781-1802.

49. G. J. Martyna, D. J. Tobias and M. L. Klein, *J. Chem. Phys.*, 1994, **101**, 4177-4189.

50. S. E. Feller, Y. Zhang, R. W. Pastor and B. R. Brooks, *J. Chem. Phys.*, 1995, **103**, 4613-4621.

51. L. Martínez, R. Andrade, E. G. Birgin and J. M. Martínez, *Journal of computational chemistry*, 2009, **30**, 2157-2164.

52. G. Stirnemann, D. Giganti, J. M. Fernandez and B. Berne, *Proc. Natl. Acad. Sci.*, 2013, **110**, 3847-3852.

53. S. De Leeuw, J. Perram and E. Smith, *Proceedings of the Royal Society of London. A. Mathematical and Physical Sciences*, 1983, **388**, 177-193.

54. H. S. Salehi, M. Ramdin, O. A. Moultos and T. J. Vlugt, *Fluid Phase Equilib.*, 2019, **497**, 10-18.

55. K. X. Huang, M. Mohan, A. George, B. A. Simmons, Y. Xu and J. M. Gladden, *Green Chem.*, 2021, **23**, 6036-6049.

56. A. Niederquell, N. Wyttenbach and M. Kuentz, *International journal of pharmaceutics*, 2018, **546**, 137-144.

57. C. Loschen and A. Klamt, *Ind. Eng. Chem. Res.*, 2012, **51**, 14303-14308.
58. M. Mohan, T. Banerjee and V. V. Goud, *ACS omega*, 2018, **3**, 7358-7370.
59. M. Mohan, V. V. Goud and T. Banerjee, *Fluid Phase Equilib.*, 2015, **395**, 33-43.
60. M. Mohan, T. Banerjee and V. V. Goud, *J. Chem. Eng. Data*, 2016, **61**, 2923-2932.
61. H. D. Magurudeniya, N. R. Baral, A. Rodriguez, C. D. Scown, J. Dahlberg, D. Putnam, A. George, B. A. Simmons and J. M. Gladden, *Green Chem.*, 2021, **23**, 3127-3140.
62. M. Mohan, H. Choudhary, A. George, B. A. Simmons, K. Sale and J. M. Gladden, *Green Chem.*, 2021, **23**, 6020-6035.
63. D. R. Lide, *CRC handbook of chemistry and physics*, CRC press, 2004.
64. K. Vanommeslaeghe, E. P. Raman and A. D. MacKerell Jr, *J. Chem. Inf. Model.*, 2012, **52**, 3155-3168.
65. CGenFF interface at paramchem.org, https://cgenff.umaryland.edu, (accessed 11-19-2021).
66. B. Sanchez-Lengeling, L. M. Roch, J. D. Perea, S. Langner, C. J. Brabec and A. Aspuru-Guzik, *Advanced Theory and Simulations*, 2019, **2**, 1800069.
67. W. Wang and D.-J. Lee, *Bioresource Technology*, 2021, 125587.
68. D. Smink, A. Juan, B. Schuur and S. R. Kersten, *Ind. Eng. Chem. Res.*, 2019, **58**, 16348-16357.
69. H. Q. Lê, A. Zaitseva, J. P. Pokki, M. Ståhl, V. Alopaeus and H. Sixta, *ChemSusChem*, 2016, **9**, 2939.
70. J. Sun, N. M. Konda, R. Parthasarathi, T. Dutta, M. Valiev, F. Xu, B. A. Simmons and S. Singh, *Green Chem.*, 2017, **19**, 3152-3163.
71. E. C. Achinivu, M. Mohan, H. Choudhary, L. Das, K. Huang, H. Magurudeniya, V. Pidatala, A. George, B. Simmons and J. M. Gladden, *Green Chem.*, 2021, DOI: 10.1039/D1GC01186C, DOI: 10.1039/D1031GC01186C.
72. A. Yao, H. Choudhary, M. Mohan, A. Rodriguez, H. Magurudeniya, J. G. Pelton, A. George, B. A. Simmons and J. M. Gladden, *ACS Sustain. Chem. Eng.*, 2021, **9**, 4371-4376.
73. B. Saha, I. Klein, T. Parsell and M. M. Abu-Omar, in *Reaction Pathways and Mechanisms in Thermocatalytic Biomass Conversion II*, Springer, 2016, pp. 119-129.
74. A. Olsson and L. Salmén, 1992.
75. Z. Börcsök and Z. Pásztory, *European Journal of Wood and Wood Products*, 2020, 1-16.
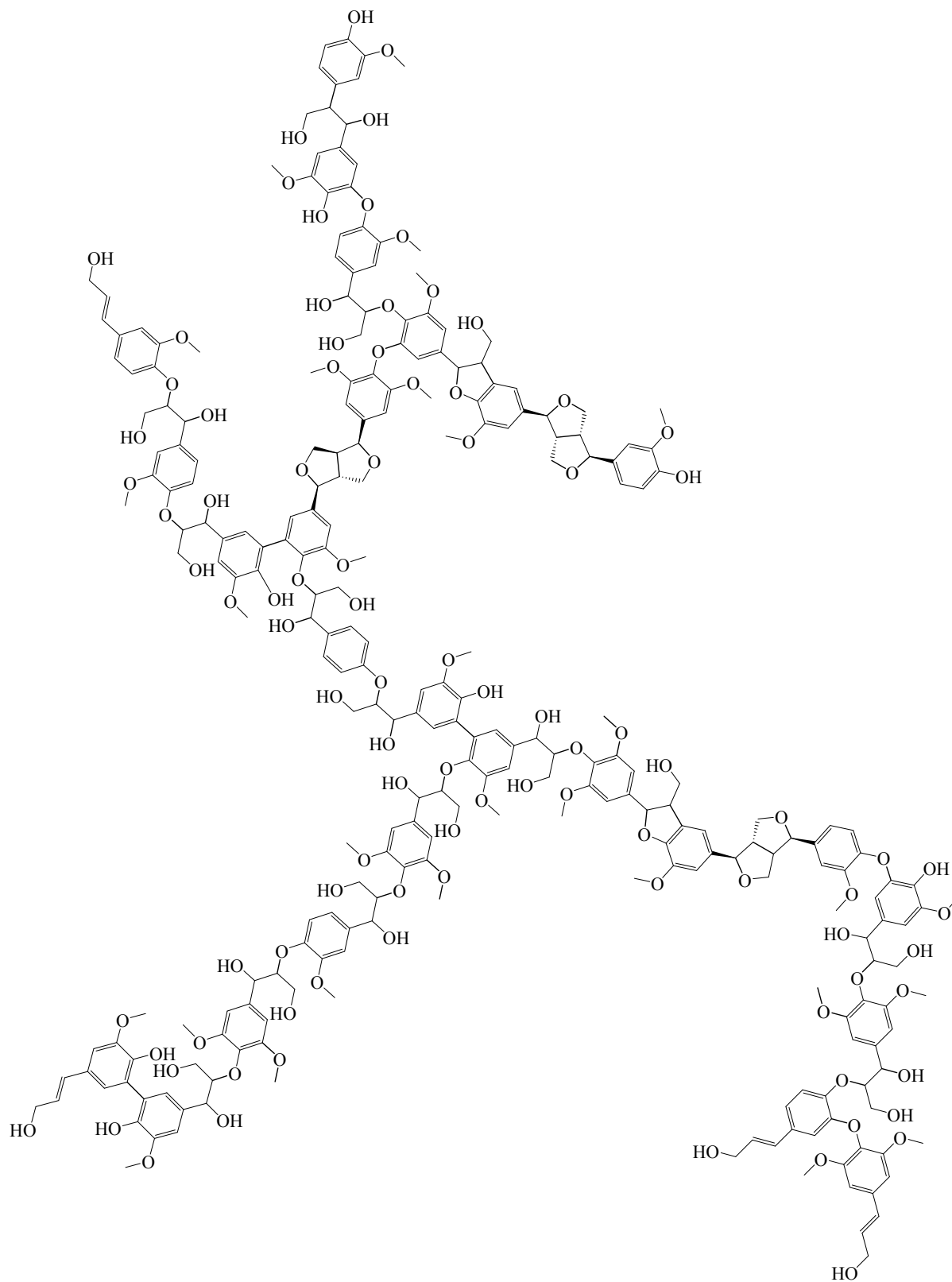76. L. Das, H. Choudhary, J. M. Gladden and B. A. Simmons, *Journal*, 2021.

Figure 1: Chemical structures of lignin (DP = 26). The lignin molecule is composed of all possible linkages such as β–β, β–1, β–5, 5–5, β–O–4, α–O–4, and 4–O–5 linkages.

Cholinium   1-ethyl-3-methylimidazolium   Formate   Acetate   Butyrate

Hexanoate   Octanoate   Lysinate

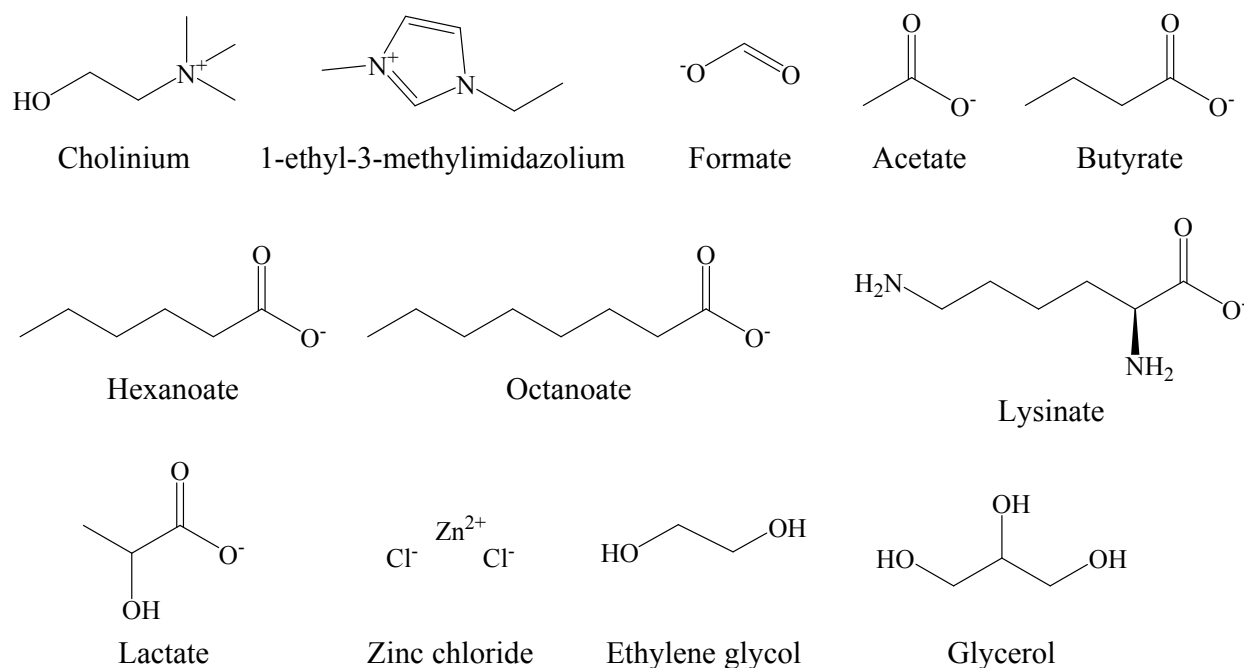Lactate   Zinc chloride   Ethylene glycol   Glycerol

Figure 2: Chemical structures of investigated cation and anions of ILs, and HBA and HBDs of mDESs.

Table 1: Solubility properties and parameters of different ILs and mDESs computed at 363.15 K from MD simulations. The listed SPs include Hildebrand and Hansen SPs and various contributors (dispersion and electrostatic) to the HSPs

Ionic Liquid/mDES	$\Delta H_{vap}(T)^a$ (kcal/mol)	CED^b (cal/mL)	Hildebrand, δ_H (MPa$^{1/2}$)	Hansen Solubility Parameter (MPa$^{1/2}$)				Predicted Model
				δ_d	δ_p	δ_h	δ_t	
[Ch][For]	40.42	302.85	35.61	18.41	29.75^c		34.99	MD Simulations
[Ch][Ace]	40.60	264.16	33.08	18.20	26.87^c		32.46	MD Simulations
[Ch][Buty]	40.84	218.79	30.25	17.99	23.58^c		29.66	MD Simulations
[Ch][Hexa]	41.61	185.93	28.08	17.63	21.14^c		27.52	MD Simulations
[Ch][Octa]	43.46	167.57	26.52	17.32	19.51^c		26.09	MD Simulations
[Ch][Lac]	45.38	261.23	33.05	18.84	27.46^c		33.30	MD Simulations
				18.37	8.40	25.49	32.53	COSMO-RS
[Ch][Lys]	41.91	175.45	27.09	16.58	20.70^c		26.52	MD Simulations
				18.49	13.50	17.46	28.80	COSMO-RS
				16.48	12.83	15.97	26.30	HSPiP (experimental)
[Emim][Ace]	42.05	269.92	33.60	19.43	27.14^c		33.38	MD Simulations
300 K^d	45.28	296.50	35.22	-	-	-	-	MD Simulations
[Emim][Lys]	40.58	166.59	26.39	17.20	19.55^c		26.03	MD Simulations
ZnCl$_2$-EG (1:4)	59.08	203.66	29.18	15.74	23.83^c		28.56	MD Simulations
ZnCl$_2$-Gly (1:3)	65.06	227.33	30.83	15.36	27.53^c		31.53	MD Simulations

^{a} ΔH_{vap} = heat of vaporization; ^{b} CED = cohesive energy density; ^{c} δ_e is the SP contribution from electrostatic term (summation of polar and hydrogen bonded); ^{d} taken from Liu et al. (2010)[26]

Table 2: Hansen solubility parameter of the solvents used for the dissolution of cholinium lysinate [Ch][Lys] and the experimental results. Score '1' means soluble and score '0' means insoluble

Solvent	δ_d	δ_p	δ_h	Score*	RED
Acetonitrile	15.3	18.0	6.1	0	1.588
Ethylene glycol	17.0	11.0	26.0	1	0.999
Dichloromethane	17.0	7.3	7.1	0	1.454
Ethanol	15.8	8.8	19.4	1	0.710
Dimethyl formamide	17.4	13.7	11.3	1	0.766
Methanol	14.7	12.3	22.3	1	0.857
Dimethyl sulfoxide	18.4	16.4	10.2	1	1.000
Propylene carbonate	20.0	18.0	4.1	0	1.822
Decane	15.7	0.0	0.0	0	2.696
1,4-dioxane	17.5	1.8	9.0	0	1.760
p-xylene	17.8	1.0	3.1	0	2.301
Ethyl acetate	15.8	5.3	7.2	0	1.632
Toluene	18.0	1.4	2.0	0	2.368
Methyl formate	15.3	8.4	10.2	0	1.194
Ethanolamine	17.0	15.5	21.0	1	0.497
1-octanol	16.0	5.0	11.2	0	1.331
Ethylene dichloride	18.0	7.4	4.1	0	1.759
2-propanol	15.8	6.1	16.4	1	0.991
1-propanol	16.0	6.8	17.4	1	0.886

* *Score: 1 – soluble (good) and 0 – insoluble (bad)*
In= 8 Out= 11 Total= 19
δ_d= 16.48 δ_p=12.83 δ_h=15.97
Tot = 26.3, Radius = 7.7
Fit= 1.000
Core= ± [0.65, 0.80, 0.40]
Wrong In= 0
Wrong Out= 0

Green Chemistry

Table 3: Solubility parameters of different ILs, Lignin dimers and polymers computed from diff. computational approaches. The listed HSPs include various contributors' dispersion, polar, and hydrogen to the HSPs.

Lignin	Hansen Solubility Parameter (MPa$^{1/2}$)				Predicted Model
	δ_d	δ_p	δ_h	δ_t	
Lignin (DP = 8)	18.70	19.07[¥]		26.71	MD Simulations
Lignin (DP = 11)	18.04	18.48[¥]		25.83	MD Simulations
Lignin (DP = 26)	16.55	16.01[¥]		23.03	MD Simulations
Hardwood Lignin	16.70	13.50	11.30	24.30	Thielemans and Wool (2005)[40]
Organosolv Lignin	-	-	-	25.5	Le et al. (2014)[69]
Lignin	21.90	14.10	16.90	31.05	Hansen (2017)[30]

[¥] δ_e is the SP contribution from electrostatic term (summation of polar and hydrogen bonded)

Table 4: Correlation between RED values of solvent (ILs)−lignin interaction and experimental lignin solubility/biomass delignification

Biomass Type	Ionic Liquid	Total HSP (δ_t) of IL	Lignin removal (%)	RED[a]	RED[b]	Reference
Kraft lignin[c]	[Ch][For]	34.99	28.3	1.04	0.92	Hou et al. (2015)[25]
	[Ch][Ace]	32.46	31	0.83	0.71	
	[Ch][But]	29.66	32.5	0.59	0.47	
	[Ch][Hex]	27.52	37.2	0.41	0.29	
	[Ch][Oct]	26.09	39.5	0.28	0.19	
Sorghum (grass)[d]	[Ch][Ace]	32.46	45	0.83	0.71	Yao et al. (2021)[72]
	[Ch][Oct]	26.09	51.86	0.28	0.17	
	[Ch][Lys]	26.43	77.41	0.34	0.22	
Switchgrass (grass)[e,f]	[Emim][Ace]	33.38	16.5[e], 48.9[f]	0.91	0.80	Sun et al. (2014)[19]
	[Ch][Ace]	32.46	17.0[e], 50.2[f]	0.83	0.71	
	[Ch][Lys]	26.52	69.3[e], 85.1[f]	0.34	0.22	
	[Emim][Lys]	26.03	80.3[e], 86.6[f]	0.28	0.16	
Switchgrass (grass)[h]	[Ch][Lys]	26.52	74	0.34	0.22	Dutta et al. (2018)[41]
Eucalyptus (hardwood)[h]	[Ch][Lys]	26.52	70	0.34	0.22	Dutta et al. (2018)[41]
Pine (softwood)[h]	[Ch][Lys]	26.52	20	-	0.79	Dutta et al. (2018)[41]

[a] RED of lignin based on the MD predicted lignin HSP values δ_d = 16.55; δ_e = 16.01; and δ_t = 23.03;
[b] RED of lignin based on the experimental (from literature) HSP values (hardwood and grass)[40] δ_d = 16.7; δ_e = 17.60; and δ_t = 24.27 and the HSP of softwood[30] lignin δ_d = 21.9; δ_e = 22.53; and δ_t = 31.6, and the radius of lignin is 13.7; the RED values of lignin are calculated based on the equation 2.
Experimental conditions: [c] Temp = 90 °C and 24 h of solubility time (t), [d] Temp = 140 °C and t = 3 h; [e] Temp = 90 °C and t = 5 h; [f] Temp = 140 °C and t = 1 h; and [h] Temp = 140 °C and t = 1 h